Journal of Computational Physics 228 (2009) 387–405

Contents lists available at ScienceDirect

Journal of Computational Physics

journal homepage: www.elsevier.com/locate/jcp

Numerical coupling of Landau damping and Raman amplification

R. Belaouar [a,b], T. Colin [b,*], G. Gallice [a]

[a] CEA CESTA, SIS, BP 2 33114 Le barp, France
[b] University Bordeaux 1 IMB, INRIA Bordeaux Sud-Ouest, EPI MC2, 351 cours de la Libération, 33405 Talence, France

ARTICLE INFO

Article history:
Received 27 February 2007
Received in revised form 4 August 2008
Accepted 19 September 2008
Available online 4 October 2008

Keywords:
Plasma physics
Landau damping
Raman instability
Numerical simulations
Zakharov systems
Stability

ABSTRACT

In this paper, we present a numerical model for laser-plasma interaction involving Raman instability and Landau damping. This model exhibits three main difficulties. The first one is the coupling of PDE's posed both in Fourier space and in physical space. The second one is a three-waves resonance condition that has to be verified. The third one is the boundary conditions. We overcome these difficulties using, respectively a splitting scheme, a numerical dispersion relation and absorbing boundary conditions. We present some comparison between several phenomena that are involved and the influence of the Raman amplification and the Landau damping.

1. Introduction and physical context

The interaction of an intense laser pulse with a plasma is a complex physical phenomenon. Numerical simulation plays a key role in its understanding. One of the main goal is to simulate nuclear fusion by inertial confinement in a laboratory. We therefore need some accurate and reliable numerical models of laser-plasma interactions. Vlasov or particle-in-cell (PIC) simulations have been used for a complete description of the problem. However, these kinetic simulations have difficulties in studying weak instabilities and long time behaviors because they need to resolve very small spatial and temporal scales. For the same reasons, it is not possible to use Euler–Maxwell equations.

Recently, Colin and Colin [5], starting from [14], derived a complete set of quasi-linear Zakharov equations describing the interactions between the laser fields, the stimulated Raman processes, the electronic plasma waves and the low-frequency variations of density of the ions. The system involves four Schrödinger equations coupled by quasi-linear terms and a wave equation and describes a three-waves interaction. Physically, the lasers interacts with the plasma, part of it backscattered through a Raman-type process to create an electron plasma wave. These three-waves interact in order to create a low-frequency variation of density which has itself an influence on the three preceding waves. However, this model that is obtained starting from the fluid equations does not take into account the kinetic effects such the Landau damping effect which is a wave-particle process which occurs in under-dense plasma. The Landau damping process is especially important in the context of fusion by inertial confinement by lasers because electrons are accelerated to high energy and this induces a preheat of the fusion fuel and reduces the target gain. This wave-particle process corresponds to a resonant effect between the electrons of the plasma and the plasma electronic waves. This effect implies an exchange of energy between electrons and the plasma waves. As a result, the plasma waves are damped.

* Corresponding author.
E-mail addresses: belaouar@cmap.polytechnique.fr (R. Belaouar), colin@math.u-bordeaux1.fr (T. Colin), gerard.gallice@cea.fr (G. Gallice).

0021-9991/$ - see front matter © 2008 Elsevier Inc. All rights reserved.
doi:10.1016/j.jcp.2008.09.019

Of course many description of the Landau damping phenomenon exists in the literature starting at the kinetic level (see Glassey–Schaeffer [11], Degond [8] for example). Here we do not try to obtain such precise models. The aim of this paper is to propose a numerical model for the coupling of Landau damping and Raman amplification. The main points of this work are: (i) we introduce a new model which is a generalization of [14,17] and that allows us to recover the main feature of both processes without using kinetic models. (ii) We provide an accurate scheme with suitable stability properties.

In order to obtain a system describing this wave-particle process we complete the system used in [5] by using the model derived in [2]. The aim of this paper is to perform mathematically and numerically the coupling of these models that describes the interaction of the variation of the density of ions with the slowly varying envelope of the plasma electronic waves, the spatial mean value of the distribution function of the electrons, the laser field and the Raman component. We want to achieve two goals. The first one is to investigate what is the influence of the Landau damping process on the saturation of the Raman amplification. The second question we want to address is the influence of the Raman instability on the model [2] in terms of the number of accelerated electrons.

For that study, we use the scheme introduced in [5], a time-splitting discretization for the Landau damping term and a implicit finite difference scheme for the distribution function of the electrons. The main difficulties are the following:

(i) First we have to couple the equations of the Raman model of [5] with those of the Landau model of [2]. This is done numerically by using a splitting strategy in Section 3.1. The Landau damping model consist in two partial differential equations, one is posed in the physical space, the other one in Fourier space. The Fourier transform of some field occurs explicitly in the partial differential equations. The coupling of such models in the context of boundary value is not obvious especially because of the electronic plasma waves hat have to be considered in a periodic framework in the model [2].

(ii) The second difficulty is the three-waves interaction condition. Indeed, it is shown in [5] that the Raman system that is obtained relies on an interaction condition. In our context, this condition means that the couple (k_1, ω_1) involved in the system is such that $e^{i(k_1 x-\omega_1 t)}$ is an exact solution to a linear Schrödinger equation. It is a phase matching condition. After discretization, one obtains a numerical phase matching condition that is different from that of the continuous case. In order to handle this difficulty, we define and use ω_{1d}, the frequency given by the numerical dispersion relation. This is done in Section 3.2.

(iii) The third difficulty is linked to the spatial box. For physical considerations, we cannot use periodic boundary conditions since we want that once a pulse (the laser part or the Raman part) hits the boundary, it does not interact anymore with the remaining part of the system. We therefore introduce some kind of absorbing boundary conditions. It is the object of Section 3.3.

The outline of the paper is the following one. Section 2 is devoted to a complete presentation of the model and we introduced a dimensionless form. In Section 3, in order to solve the problem, we introduce an effective numerical scheme and show some of its stability properties. In Section 4, we deal with the boundary conditions Finally, in the last section, we will provide some numerical results in order first to validate our methods and then to study the coupling between Raman amplification and Landau damping process and to compare the results with previous models.

2. The model and its properties

2.1. The equations and their non-dimensional form

In this section, we introduce the one-dimensional system describing the Raman amplification and the Landau damping process. We consider here an homogeneous plasma where collisions between the particles (electrons and ions) and the gravitational field are neglected. We want to describe the interaction of a laser field with this plasma and the physical phenomenon quoted previously. In the one-dimensional (y, v) phase space, we use the following model (see [5]):

$$i\left(\partial_t A_0 + \frac{k_0 c^2}{\omega_0}\partial_y A_0\right) + \frac{c^2}{2\omega_0}\left(1 - \frac{k_0^2 c^2}{\omega_0^2}\right)\partial_y^2 A_0 = \frac{\omega_{pe}^2}{2n_0\omega_0}\delta n A_0 - \frac{e}{2m_e\omega_0}(\partial_y E)A_R e^{-i(k_1 y-\omega_1 t)}, \tag{2.1}$$

$$i\left(\partial_t A_R + \frac{k_R c^2}{\omega_R}\partial_y A_R\right) + \frac{c^2}{2\omega_R}\left(1 - \frac{k_R^2 c^2}{\omega_R^2}\right)\partial_y^2 A_R = \frac{\omega_{pe}^2}{2n_0\omega_R}\delta n A_R - \frac{e}{2m_e\omega_R}(\partial_y E^*)A_0 e^{i(k_1 y-\omega_1 t)}, \tag{2.2}$$

$$i(\partial_t E + \nu * E) + \frac{3v_{the}^2}{2\omega_{pe}}\partial_y^2 E = \frac{\omega_{pe}}{2n_0}\delta n E + \frac{e\omega_{pe}}{2c^2 m_e}\partial_y(A_R^* A_0 e^{i(k_1 y-\omega_1 t)}), \tag{2.3}$$

$$(\partial_t^2 - c_s^2\partial_y^2)\delta n = \frac{1}{4\pi m_i}\partial_y^2\left(|E|^2 + \frac{\omega_{pe}^2}{c^2}(|A_0|^2 + |A_R|^2)\right), \tag{2.4}$$

$$\hat{\nu}(\xi, t) = -\frac{\pi\omega_{pe}^3}{2n_0|\xi|\xi}\partial_v F_e\left(t, \frac{\omega_{pe}}{\xi}\right), \tag{2.5}$$

$$\partial_t F_e = \partial_v(D(v, t)\partial_v F_e), D(v, t) = \frac{e^2}{2m_e^2|v|}\left|\widehat{E}\left(\frac{\omega_{pe}}{v}, t\right)\right|^2. \tag{2.6}$$

Here A_0 is the envelope of the vector potential of the incident electromagnetic laser field, A_R is the envelope of the vector potential of Raman backscattered light, E is the slowly varying amplitude of the high-frequency electronic plasma waves, δn the low-frequency variation of the density of the ions, F_e the spatially averaged electron distribution function, $\hat{v}$ the spatial fourier transform of v corresponding to the Landau damping rate and u^* is the complex conjugate of u. In this work we consider that the laser propagates in the positive y-direction and we stay in the one-dimensional framework.

This system involves three Schrödinger equations coupled by quasi-linear terms and the low-frequency fluctuation of density given by the wave equation (2.4). The electron distribution function satisfies a heat equation where the diffusion coefficient $D(v,t)$ depends on the density spectral energy of electron plasma waves. Concerning the wave-particle process, the model is valid for bounded velocities that are also bounded away from zero (see [7]). Equation (2.6) is therefore satisfied on a bounded domain Ω_v of the form $[-A,a]\cup[a,A]$. Note that the term $\hat{v}$ is *a priori* not defined on the whole line; we extend it by zero. The constants are defined by:

- c is the speed of light in the vacuum, e is the elementary electric charge,
- m_e and m_i are, respectively the electron's and ion's mass,
- n_0 is the mean background density of the plasma,
- T_e is the electronic temperature,
- ω_{pe}, v_{the} and c_s are, respectively the electronic plasma pulsation, the thermal velocity of electrons and the acoustic velocity of ions given by

$$\omega_{pe}=\sqrt{\frac{4\pi e^2 n_0}{m_e}},\quad v_{the}=\sqrt{\frac{T_e}{m_e}},\quad c_s=\sqrt{\frac{T_e}{m_i}},$$

- ω_0, ω_R, $\omega_{pe}+\omega_1$ are, respectively the laser pump frequency, the Raman component frequency and the electronic plasma wave frequency,
- k_0, k_R, k_1, are, respectively the laser pump wave number, the Raman component wave number and the electronic plasma wave number.

From the practical point of view, one starts with a non-zero value for the laser field A_0 and only noise for A_R and E. A growth of A_R and E can occur only if the exponential term $e^{i(k_1y-\omega_1t)}$ is resonant with the linear part of Eq. (2.3). That means that $(\omega_{pe}+\omega_1,k_1)$ has to satisfy the dispersion relation of the electronic plasma waves. This resonance condition (called three-waves resonance condition) means that $(\omega_0,\omega_R,\omega_1)$ and (k_0,k_R,k_1) have to satisfy

$$\omega_0=\omega_R+\omega_{pe}+\omega_1, \tag{2.7}$$
$$k_0=k_R+k_1. \tag{2.8}$$

Here (k_0,ω_0), (k_R,ω_R) correspond to electromagnetic waves while $(k_1,\omega_{pe}+\omega_1)$, corresponds to electronic plasma waves and the dispersion relations are therefore

$$\omega_0^2=\omega_{pe}^2+c^2k_0^2, \tag{2.9}$$
$$\omega_R^2=\omega_{pe}^2+c^2k_R^2, \tag{2.10}$$
$$(\omega_{pe}+\omega_1)^2=\omega_{pe}^2+3v_{the}^2k_1^2. \tag{2.11}$$

Note that, the last relation can be written approximatively $\omega_1\approx\frac{3v_{the}^2k_1^2}{2\omega_{pe}}$.

The full electric field can then be recovered as follows:

$$E_f(t,x)=i\frac{\omega_0}{c_0}A_0e^{i(k_0y-\omega_0t)}+i\frac{\omega_R}{c}A_Re^{i(k_Ry-\omega_Rt)}+Ee^{-i\omega_{pe}t}+c.c.$$

where $c.c.$ denotes the complex conjugate.

With this model, we can recover the model used in [5] by taking $v=0$ in (2.3) to obtain system (2.1)–(2.4) which was derived from a bi-fluid Euler–Maxwell system. We can also recover the system used in [2] by fixing the potentials A_R and A_0 to obtain system (2.3)–(2.6) where in (2.3), we have a fixed source term given by $\partial_y(A_R^*A_0e^{i(k_1y-\omega_1t)})$.

2.2. Dimensionless system

We now introduce a dimensionless form of (2.1)–(2.6).

We use $T=\frac{1}{\omega_0}$ as time scale and $L=\frac{1}{k_0}$ as space scale and introduce

$$\widetilde{A_0}=\frac{e}{m_ec^2}A_0,\quad \widetilde{A_R}=\frac{e}{m_ec^2}A_R,$$
$$\widetilde{E}=\frac{e}{m_ev_{the}\omega_{pe}}E,\quad \widetilde{\hat{v}}=\frac{1}{\omega_{pe}}\hat{v},$$
$$\widetilde{k_1}=\frac{k_1}{k_0},\quad \widetilde{\omega_1}=\frac{\omega_1}{\omega_0},\quad \widetilde{v}=\frac{v}{v_{the}},$$
$$\widetilde{F_e}=\frac{v_{the}}{n_0}F_e,\quad \widetilde{\delta n}=\frac{1}{n_0}\delta n.$$

Omitting the tildes, we get the following system for A_0, A_R, E, δn:

$$i(\partial_t A_0 + v_0\partial_y A_0) + \alpha_0\partial_y^2 A_0 = \beta_0\delta n A_0 - \gamma_0(\partial_y E)A_R e^{-i(k_1 y-\omega_1 t)}, \tag{2.12}$$

$$i(\partial_t A_R + v_R\partial_y A_R) + \alpha_R\partial_y^2 A_R = \beta_R\delta n A_R - \gamma_R(\partial_y E^*)A_0 e^{i(k_1 y-\omega_1 t)}, \tag{2.13}$$

$$i\left(\partial_t E + \frac{\omega_{pe}}{\omega_0} v * E\right) + \alpha_E\partial_y^2 E = \beta_E\delta n E + \gamma_E\partial_y(A_R^* A_0 e^{i(k_1 y-\omega_1 t)}), \tag{2.14}$$

$$\left(\partial_t^2 - v_s^2\partial_y^2\right)\delta n = \delta_2\partial_y^2|E|^2 + \delta_1\partial_y^2(|A_0|^2 + |A_R|^2). \tag{2.15}$$

where

$$v_0 = \frac{k_0^2c^2}{\omega_0^2}, \quad v_R = \frac{k_R k_0 c^2}{\omega_0\omega_R}, \quad v_s = \frac{c_s k_0}{\omega_0}$$

$$\alpha_0 = \frac{1}{2}v_0(1-v_0), \quad \beta_0 = \frac{\omega_{pe}^2}{2\omega_0^2}, \quad \gamma_0 = \frac{k_0\omega_{pe}^2}{2k_{De}\omega_0^2},$$

$$\alpha_R = \frac{c^2k_0^2}{2\omega_R\omega_0}\left(1 - \frac{c^2k_R^2}{\omega_R^2}\right), \quad \beta_R = \frac{\omega_{pe}^2}{2\omega_0\omega_R}, \quad \gamma_R = \frac{k_0\omega_{pe}^2}{2k_{De}\omega_0\omega_R},$$

$$\alpha_E = \frac{3k_0^2\omega_{pe}}{2k_{De}^2\omega_0}, \quad \beta_E = \frac{\omega_{pe}}{2\omega_0}, \quad \gamma_E = \frac{c^2k_0k_{De}}{2\omega_0\omega_{pe}},$$

$$\delta_1 = \frac{k_0^2c^2}{\omega_0^2}\frac{m_e}{m_i}, \quad \delta_2 = \frac{v_{the^2}}{c^2}\delta_1.$$

In these expression, $k_{De}=\frac{1}{\lambda_{De}}$ where λ_{De} denotes the Debye length given by $\lambda_{De} = \frac{v_{the}}{\omega_{pe}}$.

For the Landau damping part, one gets

$$\hat{v}(t,\xi) = -\frac{\pi k_{De}^2}{2k_0^2\xi|\xi|}\partial_v F_e\left(v = \frac{k_{De}}{k_0\xi}\right), \tag{2.16}$$

$$\partial_t F_e = \partial_v(D(v,t)\partial_v F_e), D(v,t) = \frac{k_{De}\omega_{pe}}{2k_0\omega_0|v|}\left|\widehat{E}\left(\xi = \frac{k_{De}}{k_0 v}, t\right)\right|^2. \tag{2.17}$$

In order to study the quasi-linear diffusion equation (2.17), it is more convenient to use the variable $\xi = \frac{k_{De}}{k_0 v}$. Then denoting

$$H(t,\xi) = F_e\left(t, \frac{k_{De}}{k_0\xi}\right),$$

the distribution function, (2.17) becomes

$$\partial_t H - \eta\xi^2\partial_\xi(|\xi|^3|\widehat{E}(t,\xi)|^2\partial_\xi H) = 0, \tag{2.18}$$

where $\eta = \frac{\omega_{pe}k_0^2}{\omega_0 k_{De}^2}$ and is satisfied on the domain $\Omega = [-\xi_{\max}, -\xi_{\min}] \cup [\xi_{\min}, \xi_{\max}]$. The Landau damping rate then reads

$$\hat{v}(t,\xi) = sgn(\xi)\frac{\pi}{2}\frac{k_{De}^3}{k_0^3}\partial_\xi H(t,\xi). \tag{2.19}$$

2.3. Some basic properties

One first have an energy conservation given by

Proposition 2.1. *For any regular solution of (2.12)–(2.17), one has*

$$\frac{d}{dt}\int\left(\frac{1}{\gamma_0}|A_0|^2 + \frac{1}{\gamma_R}|A_R|^2 + \frac{1}{\gamma_E}|E|^2\right)dy + \frac{2\omega_{pe}}{\omega_0\gamma_E}\int\hat{v}(t,\xi)|\widehat{E}|^2(t,\xi)d\xi = 0. \tag{2.20}$$

Proof. Multiply (2.12) by $\frac{2}{\gamma_0}A_0^*$ (2.13), by $\frac{1}{\gamma_R}A_R^*$ (2.14), by $\frac{1}{\gamma_E}E^*$, integrating over $\mathbb{R}$, summing the results, taking the imaginary part, using the Plancherel formula for the Landau damping term and denoting by $\theta = k_1 x - \omega_1 t$, give

$$\begin{aligned}
&\frac{1}{2}\frac{d}{dt}\int\left(\frac{1}{\gamma_0}|A_0|^2 + \frac{1}{\gamma_R}|A_R|^2 + \frac{1}{\gamma_E}|E|^2\right)dy + \frac{\omega_{pe}}{\omega_0\gamma_E}\int\hat{v}(t,\xi)|\widehat{E}|^2(t,\xi)d\xi \\
&\quad = \Im\int(-2\partial_y E A_R A_0^* e^{-i\theta} - \partial_y E^* A_R^* A_0 e^{i\theta} + \partial_y(A_R^* A_0 e^{i\theta})E^*)dy, \\
&\quad = \Im\int(2\partial_y E^* A_R^* A_0 e^{i\theta} - \partial_y E^* A_R^* A_0 e^{i\theta} - A_R^* A_0\partial_y E^* e^{i\theta})dy = 0. \qquad \square
\end{aligned}$$

Moreover, one has some maximum principle on (2.17) that shows that the convolution term in (2.14) is indeed a damping term. More precisely, we recall the following result imported from [2]:

Proposition 2.2. *If $\hat{v}(0,\xi) \geqslant 0$ for all ξ, then one have*

$$\hat{v}(t,\xi) = sgn(\xi)\partial_\xi H(t,\xi) \geqslant 0,$$

for all $\xi \in \mathbb{R}$ and $t > 0$.

Remark 2.1. If the initial distribution function of the electrons is a Maxwellian then one has $\hat{v}(0,\xi) \geqslant 0$. Proposition (2.1) expresses the decay of the electromagnetic energy due to the Landau damping process between the electron plasma waves and the electrons.

3. Numerical approximation

In this section, we present an numerical scheme for system (2.12)–(2.17) endowed with the following initial conditions

$$A_0(0,y) = A_{00}(y), \quad A_R(0,y) = A_{R0}(y), \quad E(0,y) = E_0(y), \tag{3.1}$$
$$\delta n(0,y) = \delta n_0(y), \quad \partial_t \delta n(0,y) = \delta n_1(y), \quad H(0,\xi) = H_0(\xi). \tag{3.2}$$

We work on the spatial domain $[0, L]$ and we use a regular mesh in space. The spatial mesh size is $\delta y = L/N$ for $N = 2M$ being an even number, the time step being $\delta t > 0$ and let the grid points and the time step be

$$y_j = j\delta y, \quad t_k = k\delta t, \quad j = 0,1,\ldots,N, \quad k = 0,1,2\ldots$$

with $y_0 = 0$ and $y_N = L$. Since we use the fast Fourier transform in order to compute $\widehat{E}$, the mesh in the y variable induces a mesh for ξ variable. We therefore define $\left(\xi_j = \frac{2\pi j}{L}\right)_{j=-N/2,\ldots,0,\ldots N/2-1}$, the frequency mesh. It is therefore natural to take $\xi_{\min} = \xi_1$ and $\xi_{\max} = \frac{2\pi(N/2-1)}{L}$. Furthermore, let A_{0j}^k, A_{Rj}^k, E_j^k, δn_j^k, and $\hat{v}_j^k$ be the approximations of $A_0(t_k,x_j)$, $A_R(t_k,x_j)$, $E(t_k,x_j)$, $\delta n(t_k,x_j)$, $\hat{v}(t_k,\xi_j)$. Then, in order to be consistent with the evaluation of $\hat{v}(t_k,\xi_j) = sgn(\xi_j)\partial_\xi H(t_k,\xi_j)$ by a centered finite difference scheme, we approximate H on the grid $(\xi_{j+\frac{1}{2}})$ defined by $\xi_{j+\frac{1}{2}} = \frac{2\pi(j+1/2)}{L}$. The relationship between E_j^k and its discrete Fourier coefficient $\widehat{E}_l^k$ is

$$E_j^k = \sum_{l=-M}^{M-1} \widehat{E}_l^k e^{i\xi_l x_j}, \quad \text{for } j = 1,\cdots N, \tag{3.3}$$

The numerical scheme used in [14] for the wave part of our model is a pseudo-spectral discretization. The authors observed some aliasing errors due to the nonlinear and quasi-linear terms and they were obliged to truncate the Fourier transform of the different fields. In [6], a fractional-step, Crank–Nicolson-type scheme with relaxation directly inspired by that of Besse for NLS (see [4]) is proposed for the quasi-linear system. For the acoustic part, they used an energy-preserving finite difference scheme introduced by Glassey (see [10]).

We present our scheme in three parts. In the first part, we give the scheme in itself in the case of periodic boundary condition (Section 3.1). In the second part, we present some stability result (Section 3.2). In the third part, we deal with the three-waves resonance conditions and we explain how we overcome this difficulty (Section 3.3). In the fourth part, we explain how one can construct some kind of transparent boundary conditions for our problem (Section 4).

3.1. The numerical scheme

The Landau damping rate in equation (2.14) is given by the diffusion equation (2.18) in Fourier space while the Zakharov part (2.12)–(2.15) is posed in the physical space. Therefore we have to use a spectral method to evaluate this convolution operator. In the other hand we cannot use a spectral method for the linear part of (2.12) and (2.13) since we deal with transport operators. To overcome this difficulty, we introduce a splitting technique on the Landau damping process in order to separate the Raman amplification process and the Landau damping. Therefore, as we will see in numerical applications, since the group velocity of the electronic plasma waves is closed to zero, this allows us to use a spectral method (periodic boundary conditions for E) to solve the Landau damping part. Finally, for the Raman amplification, we use the numerical scheme introduced in [6]. We now describe more precisely the different step of our method. If at time t^k, we know A_{0j}^k, A_{Rj}^k, E_j^k, δn_j^k, $H_{j+\frac{1}{2}}^k$ and $\hat{v}_j^k$, we construct A_{0j}^{k+1}, A_{Rj}^{k+1}, E_j^{k+1}, δn_j^{k+1}, $H_{j+\frac{1}{2}}^{k+1}$ and $\hat{v}_j^{k+1}$ in three steps.

In a first step, we use a scheme for the quasi-linear diffusion equation. In a second one, we introduce the scheme used in [6] for (2.12)–(2.15) without the convolution operator describing the Landau process and finally, using a fast Fourier transform, we compute the modification given by the Landau damping rate on the electronic plasma waves.

Step 1: The diffusion. In order to evaluate the approximation of $H(t_k,\xi_{j+\frac{1}{2}})$, we use an implicit difference scheme for the diffusion equation:

$$\partial_t H - \eta\xi^2\partial_\xi(|\xi|^3|\widehat{E}|^2\partial_\xi H) = 0, \xi \in \Omega = [-\xi_{\max}, -\xi_{\min}] \cup [\xi_{\min}, \xi_{\max}],$$

Concerning the boundary conditions for the distribution H, we used the same one that in [3]. At points $\xi = \pm\xi_{\min}$ corresponding to the highest discrete velocities $v = \pm\frac{k_{De}}{k_0\xi_{\min}}$, in order to simulate electron's heating due to the diffusion, we use homogeneous Neumann boundary conditions (in practice $\frac{k_{De}}{k_0\xi_{\min}} \sim 10$). At points $\xi = \pm\xi_{\max}$ corresponding to the smallest discrete velocities $v = \pm\frac{k_{De}}{k_0\xi_{\max}}$, the physic established in [14–17] shows that the distribution function does not evolved with time at these points. Therefore we fixed the distribution $H(t, \pm\xi_{\max})$ at its initial value $H(0, \pm\xi_{\max})$ (in practice $\frac{k_{De}}{k_0\xi_{\max}} \sim 1$). So, we used the following boundary conditions: $\forall t \geqslant 0$

$$\partial_\xi H(t, \pm\xi_{\min}) = 0, \tag{3.4}$$
$$H(t, -\xi_{\max}) = H(0, -\xi_{\max}), \tag{3.5}$$
$$H(t, \xi_{\max}) = H(0, \xi_{\max}). \tag{3.6}$$

The finite difference scheme reads:

$$\frac{1}{\delta t}\left(H^{k+1}_{j+\frac{1}{2}} - H^k_{j+\frac{1}{2}}\right) + \eta(AH)^{k+1}_{j+\frac{1}{2}} = 0, \tag{3.7}$$

where $(AH)^{k+1}_{j+\frac{1}{2}}$ is a discretization of $-\xi^2\partial_\xi(|\xi|^3|\hat{E}|^2)\partial_\xi H)$ in a conservative form at the point $\xi_{j+\frac{1}{2}}$ and time t_{k+1}. We choose A such that:

$$(AH)^{k+1}_{j+\frac{1}{2}} = -\frac{\xi^2_{j+\frac{1}{2}}}{\xi_{j+1} - \xi_j}\left[\beta^k_{j+1}\frac{H^{k+1}_{j+\frac{3}{2}} - H^{k+1}_{j+\frac{1}{2}}}{\xi_{j+\frac{3}{2}} - \xi_{j+\frac{1}{2}}} - \beta^k_j\frac{H^{k+1}_{j+\frac{1}{2}} - H^{k+1}_{j-\frac{1}{2}}}{\xi_{j+\frac{1}{2}} - \xi_{j-\frac{1}{2}}}\right], \tag{3.8}$$

where β^k_j is an approximation of $|\xi|^3|\widehat{E}|^2$ at time t^k. Note that coefficient β^k in (3.8) is known and equation (3.7) is linear in H^{k+1}. Then, with this scheme, we can evaluate $\hat{v}(\xi_j, t^{k+1})$ on the frequency grid with the following centered finite difference scheme:

$$\hat{v}^{k+1}_j = sgn(\xi_j)\frac{H^{k+1}_{j+\frac{1}{2}} - H^{k+1}_{j-\frac{1}{2}}}{\xi_{j+\frac{1}{2}} - \xi_{j-\frac{1}{2}}}. \tag{3.9}$$

As shown in [2], one takes

$$\beta^k_j = \frac{\xi^2_{j+\frac{1}{2}}\xi^2_{j-\frac{1}{2}}}{|\xi_{j+\frac{1}{2}} + \xi_{j-\frac{1}{2}}|}\left|\widehat{E}^k_j\right|^2$$

in order to ensure the following conservation relation

$$\sum_j \frac{1}{\xi^4_{j+\frac{1}{2}}}H^{k+1}_{j+\frac{1}{2}} = \sum_j \frac{1}{\xi^4_{j+\frac{1}{2}}}H^k_{j+\frac{1}{2}} + \delta t\sum_j \hat{v}^{k+1}_j\left|\widehat{E}^k_j\right|^2 \tag{3.10}$$

which corresponds to the energy exchange between electrons and the electronics plasma waves. One also have a numerical maximum principle for $\hat{v}$. If $\hat{v}_0$ satisfies

$$\hat{v}_0(\xi_j) \geqslant 0, \quad j = -\frac{N}{2}, \ldots, \frac{N}{2} - 1,$$

then for all $k > 0$

$$\hat{v}^k_j \geqslant 0, \quad j = -\frac{N}{2}, \ldots, \frac{N}{2} - 1. \tag{3.11}$$

In order to illustrate how the quasi-linear diffusion works on the solution, we have computed the diffusion equation with a diffusion coefficient given by a fixed electric field

$$E(t,x) = e^{i(k_1x - \omega_1 t)}e^{-\frac{\left(x-\frac{L}{2}\right)^2}{2\triangle L^2}},$$

with $L = 2000$, $\triangle L = 50$ and $k_1 = 0.45$. The initial electron distribution function is assumed to be a Maxwellian,

$$F_{e0}(v) = \frac{1}{\sqrt{2\pi}}\exp\left(-\frac{v^2}{2}\right)$$

which gives the following initial condition for the Landau damping rate

$$\hat{v}(0,\xi) = \sqrt{\frac{\pi}{8}}\frac{1}{|\xi|^3}e^{-\frac{1}{2\xi^2}}.$$

We can remark on Fig. 1 that the electron distribution function is flattened near the phase velocity $v_\phi = \frac{1}{k_1} = 2.22$ and since the Landau damping rate depends on the slope of the electron distribution, we can see that $\widehat{\nu}$ tends toward zero near $\xi = k_1$. We will see in Section 5, what happens when we take into account the time evolution of the diffusion coefficient.

Step 2: The Raman amplification. For the Raman amplification, we introduce a fractional-step, Crank–Nicolson-type scheme with relaxation introduced by of Besse for NLS equation (see [4]). For the acoustic part, we use the scheme introduced by Glassey (see [10]). This allows us to compute the values A_0^{k+1}, A_R^{k+1}, δn^{k+1} of A_0, A_R and δn at time t^{k+1} as well as an intermediate value $E_\#^{k+1}$ of E at time $k+1$. This value $E_\#^{k+1}$ will be used as initial datum for the last step of the splitting. We consider centered discretization for each spatial differential operator. Therefore, ∂_y is approximated by the centered finite difference operator D_0:

$$(D_0 E)_i = \frac{E_{i+1} - E_{i-1}}{2\delta y},$$

and ∂_y^2 by D_+D_-:

$$(D_+D_-E)_i = \frac{E_{i+1} - 2E_i + E_{i-1}}{\delta y^2}.$$

For this first step of the splitting, the scheme reads:

$$i\frac{A_0^{k+1} - A_0^k}{\delta t} + (iv_0 D_0 + \alpha_0 D_+D_-)\left(\frac{A_0^{k+1} + A_0^k}{2}\right) = \beta_0\left(\frac{\delta n^{k+1} + \delta n^k}{2}\right)\left(\frac{A_0^{k+1} + A_0^k}{2}\right) - \frac{\gamma_0}{2}\phi^{k+\frac{1}{2}}\left(\frac{A_R^{k+1} + A_R^k}{2}\right)e^{-i\theta^{k+\frac{1}{2}}} - \frac{\gamma_0}{2}\psi^{k+\frac{1}{2}}\left(\frac{D_0E_\#^{k+1} + D_0E^k}{2}\right)e^{-i\theta^{k+\frac{1}{2}}}, \tag{3.12}$$

$$i\frac{A_R^{k+1} - A_R^k}{\delta t} + (iv_R D_0 + \alpha_R D_+D_-)\left(\frac{A_R^{k+1} + A_R^k}{2}\right) = \beta_R\left(\frac{\delta n^{k+1} + \delta n^k}{2}\right)\left(\frac{A_R^{k+1} + A_R^k}{2}\right) - \gamma_R(\phi^{k+\frac{1}{2}})^*\left(\frac{A_0^{k+1} + A_0^k}{2}\right)e^{i\theta^{k+\frac{1}{2}}}, \tag{3.13}$$

$$i\frac{E_\#^{k+1} - E^k}{\delta t} + \alpha_E D_+D_-\left(\frac{E_\#^{k+1} + E^k}{2}\right) = \beta_E\left(\frac{\delta n^{k+1} + \delta n^k}{2}\right)\left(\frac{E_\#^{k+1} + E^k}{2}\right) + \gamma_E D_0\left[\left(\psi^{k+\frac{1}{2}}\right)^*\left(\frac{A_0^{k+1} + A_0^k}{2}\right)e^{i\theta^{k+\frac{1}{2}}}\right], \tag{3.14}$$

$$\frac{\delta n^{k+1} - 2\delta n^k + \delta n^{k-1}}{\delta t^2} - v_s^2 D_+D_-\left(\frac{\delta n^{k+1} + \delta n^{k-1}}{2}\right) = \delta_2 D_+D_-(|E^k|^2) + \delta_1 D_+D_-(|A_0^k|^2 + |A_R^k|^2), \tag{3.15}$$

for the time step of length δt.

The auxiliary functions ϕ and ψ are given by

$$\frac{\phi^{k+\frac{1}{2}} + \phi^{k-\frac{1}{2}}}{2} = D_0E^k, \quad \frac{\psi^{k+\frac{1}{2}} + \psi^{k-\frac{1}{2}}}{2} = A_R^k. \tag{3.16}$$

$\phi^{k+\frac{1}{2}}$ and $\psi^{k+\frac{1}{2}}$ are prediction, respectively of $\partial_y E$ and A_R at time $t^{k+1/2} = \left(k+\frac{1}{2}\right)\delta t$. Moreover the value $\phi^{-\frac{1}{2}}$ and $\psi^{-\frac{1}{2}}$ are obtained by explicit integration of the system on one half-time step backward.

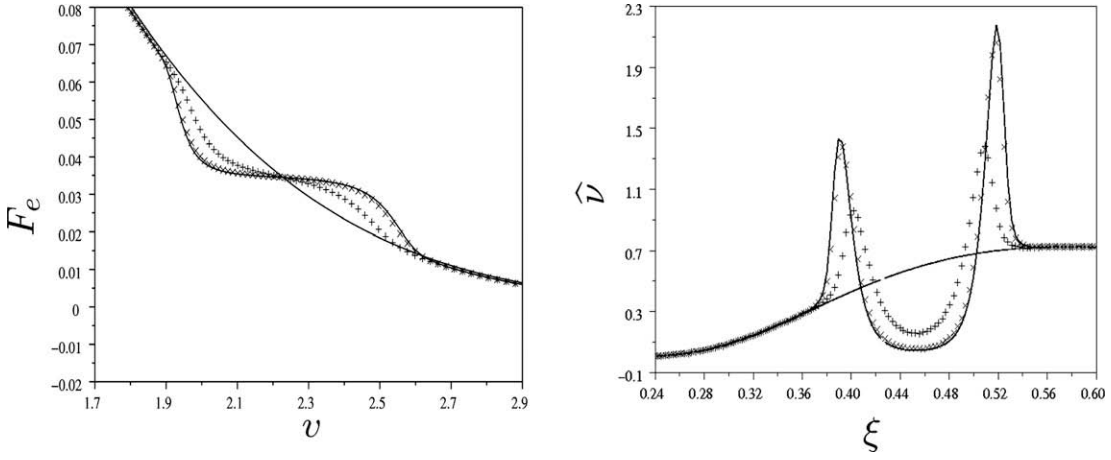

Fig. 1. The left plot corresponds to the electron distribution function F_e at different time in function of the velocity v and the right plot corresponds to the Landau damping rate $\widehat{\nu}$ at different time in function of the frequency ξ.

The discretization of the phase $\theta^{k+\frac{1}{2}}$ is given by

$$\theta^{k+\frac{1}{2}} = k_1 y - \omega_1 t^{k+1/2}.$$

Step 3: The Landau For the last step, we take

$$\widehat{E}^{k+1}(\xi_j) = \widehat{E}^{k+1}_{\#}(\xi_j)\exp\left(-\frac{\delta t}{2}\left(\hat{v}_j^{k+1} + \hat{v}_j^{k}\right)\right). \tag{3.17}$$

The values of E_j^{k+1} are recovered by an inverse fast Fourier transform.

3.2. L^2 stability result

The first stability result concerns the semi-discretization in time of the model. This semi-discretization in time is obtained by discretization of (2.12)–(2.17) only in time and using the same time-splitting as described before. It is obtained by replacing the discrete operators in space by their counterpart in the previous paragraph. We keep the same notations for the unknowns that denotes in this section the semi-discretized version of A_0, A_R, E, v, δn.

We are able to prove a stability result for the semi-discrete scheme:

Proposition 3.1. *(L^2 stability) If the initial data v^0 satisfy $\widehat{v^0}(\xi) \geqslant 0$ for all ξ, then for all $k > 0$, any solution $\left(A_0^k, A_R^k, E^k\right)$ given by the semi-discrete scheme satisfies*

$$\int_{\mathbb{R}}\left(2\frac{1}{\gamma_0}|A_0^k|^2 + \frac{1}{\gamma_R}|A_R^k|^2 + \frac{1}{\gamma_E}|E^k|^2\right)dy \leqslant \int_{\mathbb{R}}\left(2\frac{1}{\gamma_0}|A_0^0|^2 + \frac{1}{\gamma_R}|A_R^0|^2 + \frac{1}{\gamma_E}|E^0|^2\right)dy.$$

This result is the discrete version of proposition (2.1). Note that the last term in (2.20) $\frac{2\omega_{pe}}{\omega_0\gamma_E}\int \hat{v}(t,\xi)|\widehat{E}|^2(t,\xi)d\xi$ is non-negative. Unfortunately, we are not able to obtain the exact counterpart of this term. We are only able to prove (see lemma 3.1 below) that $v^k \geqslant 0$ and therefore we only prove that the step of the splitting devoted to the computation of the Landau damping decrease the energy and we obtain that the energy of the electromagnetic part is decreasing.

Proof. Using (3.17) and the Parseval formula for E^{k+1}, we have

$$\int_{\mathbb{R}}\frac{2}{\gamma_0}\left|A_0^{k+1}\right|^2 + \frac{1}{\gamma_R}\left|A_r^{k+1}\right|^2 + \frac{1}{\gamma_E}|E^{k+1}|^2 dy = \int_{\mathbb{R}}\frac{2}{\gamma_0}\left|A_0^{k+1}\right|^2 + \frac{1}{\gamma_R}\left|A_R^{k+1}\right|^2 dy + \frac{1}{\gamma_E}\int_{\mathbb{R}}\left|\widehat{E_{\#}^{k+1}}\right|^2 \exp(-\delta t(\hat{v}^k(\xi) + \hat{v}^{k+1}(\xi)))d\xi. \tag{3.18}$$

In order to conclude, we need the following version of the maximum principle.

Lemma 3.1. *If $\hat{v}^0(\xi) \geqslant 0$ for all ξ, then for all $k > 0$, any solution $\hat{v}^k$ of (3.7)–(3.9) satisfy $\hat{v}^k(\xi) \geqslant 0$ for all ξ.*

Proof. See [2]. Using the lemma 3.1 and again the Parseval formula, one gets

$$\int_{\mathbb{R}}\frac{2}{\gamma_0}\left|A_0^{k+1}\right|^2 + \frac{1}{\gamma_R}\left|A_R^{k+1}\right|^2 + \frac{1}{\gamma_E}|E^{k+1}|^2 dy \leqslant \int_{\mathbb{R}}\frac{2}{\gamma_0}\left|A_0^{k+1}\right|^2 + \frac{1}{\gamma_R}\left|A_R^{k+1}\right|^2 + \frac{1}{\gamma_E}\left|E_{\#}^{k+1}\right|^2 dy. \tag{3.19}$$

In order to conclude, we need to prove that

$$\int_{\mathbb{R}}\frac{2}{\gamma_0}\left|A_0^{k+1}\right|^2 + \frac{1}{\gamma_R}\left|A_R^{k+1}\right|^2 + \frac{1}{\gamma_E}\left|E_{\#}^{k+1}\right|^2 dy = \int_{\mathbb{R}}\frac{2}{\gamma_0}\left|A_0^{k}\right|^2 + \frac{1}{\gamma_R}\left|A_R^{k}\right|^2 + \frac{1}{\gamma_E}|E^{k}|^2 dy.$$

To this aim, we compute

$$\frac{2}{\gamma_0}\int_{\mathbb{R}}(3.12)\left(\frac{A_0^{k+1}+A_0^k}{2}\right)^* + \frac{1}{\gamma_R}\int_{\mathbb{R}}(3.13)\left(\frac{A_R^{k+1}+A_R^k}{2}\right)^* + \frac{1}{\gamma_E}\int_{\mathbb{R}}(3.14)\left(\frac{E_{\#}^{k+1}+E^k}{2}\right)^*,$$

and take the imaginary part. This yields

$$\begin{aligned}
&\frac{1}{2\delta t}\int_{\mathbb{R}}\left(\frac{2}{\gamma_0}\left|A_0^{k+1}\right|^2 + \frac{1}{\gamma_R}\left|A_R^{k+1}\right|^2 + \frac{1}{\gamma_E}\left|E_{\#}^{k+1}\right|^2\right) - \frac{1}{2\delta t}\int_{\mathbb{R}}\left(\frac{2}{\gamma_0}\left|A_0^{k}\right|^2 + \frac{1}{\gamma_R}\left|A_R^{k}\right|^2 + \frac{1}{\gamma_E}|E^{k}|^2\right)\\
&= -\mathrm{Im}\int_{\mathbb{R}}\phi^{k+\frac{1}{2}}\left(\frac{A_R^{k+1}+A_R^k}{2}\right)e^{-i\theta^{k+\frac{1}{2}}}\left(\frac{A_0^{k+1}+A_0^k}{2}\right)^* - \mathrm{Im}\int_{\mathbb{R}}\psi^{k+\frac{1}{2}}\left(\frac{\partial_y E_{\#}^{k+1}+\partial_y E^k}{2}\right)e^{-i\theta^{k+\frac{1}{2}}}\left(\frac{A_0^{k+1}+A_0^k}{2}\right)^*\\
&\quad - \mathrm{Im}\int_{\mathbb{R}}\left(\phi^{k+\frac{1}{2}}\right)^*\left(\frac{A_0^{k+1}+A_0^k}{2}\right)e^{i\theta^{k+\frac{1}{2}}}\left(\frac{A_R^{k+1}+A_R^k}{2}\right)^* + \mathrm{Im}\int_{\mathbb{R}}\partial_y\left(\left(\psi^{k+\frac{1}{2}}\right)^*\left(\frac{A_0^{k+1}+A_0^k}{2}\right)e^{i\theta^{k+\frac{1}{2}}}\right)\left(\frac{E_{\#}^{k+1}+E^k}{2}\right)^*\\
&= -\mathrm{I} - \mathrm{II} - \mathrm{III} + \mathrm{IV}.
\end{aligned}$$

It is clear that I = −III. Moreover

$$\mathrm{IV} = -\mathrm{Im}\int_{\mathbb{R}} \left(\psi^{k+\frac{1}{2}}\right)^* \left(\frac{A_0^{k+1}+A_0^k}{2}\right) e^{i\theta^{k+\frac{1}{2}}} \partial_y \left(\frac{E_\#^{k+1}+E^k}{2}\right)^* = \mathrm{II}.$$

The result follows. □

Proposition 3.1 holds for the full discretization of the system in a periodic framework. This can be shown by using the fact that if we assume $\hat{v}(t,\xi) = 0$ for all (t,ξ), then it is shown in [6] that any solution of (3.12)–(3.14) satisfies

$$\frac{2}{\gamma_0}\left|A_0^k\right|_2^2 + \frac{1}{\gamma_R}\left|A_R^k\right|_2^2 + \frac{1}{\gamma_E}|E^k|_2^2 = \frac{2}{\gamma_0}|A_{00}|_2^2 + \frac{1}{\gamma_R}|A_{R0}|_2^2 + \frac{1}{\gamma_E}|E_0|_2^2,$$

where

$$|f|_2^2 = \sum_{j=1}^{N} |f_j|^2$$

is the l^2 discrete norm. In our case, we have to include the Landau damping term $\hat{v}(t,\xi)$. The key point is that we have used a time-splitting discretization which allows us to write

$$\frac{2}{\gamma_0}\left|A_0^{k+1}\right|_2^2 + \frac{1}{\gamma_R}\left|A_R^{k+1}\right|_2^2 + \frac{1}{\gamma_E}\left|E_\#^{k+1}\right|_2^2 = \frac{2}{\gamma_0}\left|A_0^k\right|_2^2 + \frac{1}{\gamma_R}\left|A_R^k\right|_2^2 + \frac{1}{\gamma_E}\sum_{j=1}^{N}\left|E_j^{k+1}\right|^2. \tag{3.20}$$

By using twice the Parseval formula, the maximum principle (3.11) and (3.17), we obtain that

$$\sum_{j=1}^{N}\left|E_j^{k+1}\right|^2 \leqslant \sum_{j=1}^{N}\left|E_{\#j}^{k+1}\right|^2$$

and the result follows.

3.3. The three wave resonance condition

As noted in the introduction, we expect a growth on A_R which corresponds to the decomposition of the laser A_0 into a backscattered electromagnetic wave A_R and an electronic plasma waves E. The classical matching conditions for this three-waves resonance interactions is

$$k_0 = k_R + k_1, \omega_0 = \omega_R + \omega_{pe} + \omega_1,$$

where

$$\omega_0^2 = \omega_{pe}^2 + k_0^2c^2, \omega_R^2 = \omega_{pe}^2 + k_R^2c^2(\omega_{pe}+\omega_1)^2 = \omega_{pe}^2 + 3v_{the}^2k_1^2.$$

As recalled in the introduction and since $\omega_1 \ll \omega_{pe}$ (see [5]), this last condition implies $\omega_1 \approx \frac{3}{2}\omega_{pe}(k_1\lambda_{De})^2$ where $\lambda_{De} = \frac{v_{the}}{\omega_{pe}}$ is the Debye's length.

This means that (k_1,ω_1) satisfies the dispersion relation of the linear part of (2.14) and therefore the term $A_R^*A_0e^{i(k_1y-\omega_1t)}$ is resonant with the left-hand-side of (2.14) and E will grow linearly int time. If this relation is not satisfied, E will not grow and the instability does not take place see [6]. This is true at the discrete level: (k_1,ω_1) has to satisfy the dispersion relation of the left-hand-side of the numerical scheme (3.14). This discrete dispersion relation reads

$$\omega_1 = \frac{2}{\delta t}\arctan\left(\alpha_E\delta t\frac{1-\cos(k_1\delta y)}{\delta y^2}\right). \tag{3.21}$$

We will see in the numerical result section that this modification of the dispersion relation is crucial.

4. The boundary conditions

For physical considerations, we use absorbing boundary conditions for A_0 and A_R and δn. A lot of work involving transparent boundary conditions are available (see for example Di Menza [9], X. Antoine-C. Besse [1,12] for a review). Here we take into account the particular physical setting and we use a very simple version of absorbing boundary conditions. In fact, in order to model a realistic plasma slab, non-periodic boundary conditions in (3.12) and (3.13) are imposed. This condition will ensure that if the Raman backscattered field, the laser field and the density fluctuation leave the simulation box no reflection can influence the propagation of the laser field and the growth of the Raman field. It appears physically that it is very important to impose absorbing boundary conditions for A_0 and A_R and δn. In order to explain our choice of boundaries conditions, we introduce two simple independent (one for the Raman and laser fields and one for the density fluctuation) models on which one can explain our strategy.

4.1. Boundary condition for the Schrödinger equation

For the first model, we focus on the equations involving the laser potential and the Raman backscattered potential:

$$i(\partial_t A_0 + v_0\partial_y A_0) + \alpha_0\partial_y^2 A_0 = \frac{\omega_{pe}^2}{2\omega_0^2}\delta n A_0 - \frac{k_0}{k_{De}}\frac{\omega_{pe}^2}{\omega_0^2}(\partial_y E)A_R e^{-i(k_1 y-\omega_1 t)}, \tag{4.1}$$

$$i(\partial_t A_R + v_R\partial_y A_R) + \alpha_R\partial_y^2 A_R = \frac{\omega_{pe}^2}{2\omega_R\omega_0}\delta n A_R - \frac{k_0}{k_{De}}\frac{\omega_{pe}^2}{\omega_0\omega_R}(\partial_y E^*)A_0 e^{i(k_1 y-\omega_1 t)}, \tag{4.2}$$

where $\alpha_0 = \frac{1}{2}v_0(1-v_0)$ and $\alpha_R = \frac{\omega_0}{2\omega_R}\left(1-\frac{c^2k_R^2}{\omega_R^2}\right)$. The key point is that in physical applications, $|v_0|$ and $|v_R|$ are close and the dispersion coefficient α_0, α_R are closed to zero ($\alpha_{0,R}\approx 10^{-3}$). It follows that the linear part of equations (4.1) and (4.2) is a dispersive perturbation of a linear transport equation (see [5,6]). Therefore we will focus on the following Schrödinger equation

$$i(\partial_t u + \partial_y u) + \varepsilon\partial_y^2 u = 0, \quad 0 \leqslant y \leqslant 1, \tag{4.3}$$

$$u(t,0) = 0, \tag{4.4}$$

$$u(0,y) = u_0(y), \tag{4.5}$$

where ε a small positive parameter that can denote successively α_0 or α_R. The goal of this study is to give an effective absorbing boundary condition for (4.3)–(4.5) at point $y = 1$ (for A_R, one has to make a symmetry with respect to $y = 1/2$ since $v_R < 0$). Since we deal with dispersive perturbation of a transport equation, the natural choice is to impose that the solution satisfies the transport equation at point $y = 1$,

$$(\partial_t + \partial_y)u(t,1) = 0. \tag{4.6}$$

It is not clear if this boundary condition is an absorbing boundary condition. The following proposition ensure this.

Proposition 4.1. *Any solution u of (4.3), (4.4), (4.5) and (4.6) satisfies*

$$\frac{d}{dt}\int |\partial_y u|^2 dy = -(|\partial_y u(t,0)|^2 + |\partial_y u(t,1)|^2). \tag{4.7}$$

Proof. By multiplying the equation (4.3) by $\partial_t u^*$, integrating in space, taking the real part, and integrating by part the dispersive term, we get

$$Re\int i\partial_y u\partial_t u^* dy - \frac{\varepsilon}{2}\frac{d}{dt}\int |\partial_y u|^2 dy + \varepsilon Re(\partial_y u(t,1)\partial_t u^*(t,1)) = 0 \tag{4.8}$$

since $\partial_t u(t,0) = 0$. Now using the boundary condition (4.6), and plugging $i\partial_t u^* = -i\partial_y u^* + \varepsilon\partial_y^2 u^*$ in the first term of (4.7), we get

$$\varepsilon Re\int \partial_y u\partial_y^2 u^* - \frac{\varepsilon}{2}\frac{d}{dt}\int |\partial_y u|^2 dy - \varepsilon|\partial_y u(t,1)|^2 = 0. \tag{4.9}$$

and the result follows since $\varepsilon Re\int \partial_y u\partial_y^2 u^* = \frac{\varepsilon}{2}|\partial_y u(t,1)|^2 - \frac{\varepsilon}{2}|\partial_y u(t,0)|^2$. □

Remark 4.1. Using Poincare's lemma, proposition 4.1 expresses the fact that with the boundary condition (4.6), the energy (L^2-norm) decreases with time. Therefore, the estimate (4.7) show us that we can define the boundary trace of $\partial_y u$ at points $y = 0$ and $y = 1$.

For the numerical counterpart of this proposition, we use a Crank–Nicolson type scheme for (4.3)–(4.6). With the notations previously used, the scheme reads

$$i\frac{u_j^{k+1}-u_j^k}{\delta t} + (iD_0 + \varepsilon D_+D_-)\left(\frac{u^{k+1}+u^k}{2}\right)_j = 0, \quad \text{for } 2 \leqslant j \leqslant N-1. \tag{4.10}$$

We discretize the boundary condition (4.6) by using the following discretization of the linear transport equation

$$\frac{u_N^{k+1}-u_N^k}{\delta t} + D_+\left(\frac{u^{k+1}+u^k}{2}\right)_N = 0. \tag{4.11}$$

We have a discrete version of proposition 4.1

Proposition 4.2. *Any solution u^k of (4.10) and (4.11) satisfies*

$$\frac{\delta y}{\delta t}\left(\sum_{j=2}^{N-1}\left|\frac{u_{j+1}^{k+1}-u_j^{k+1}}{\delta y}\right|^2 - \sum_{j=2}^{N-1}\left|\frac{u_{j+1}^{k}-u_j^{k}}{\delta y}\right|^2\right) = -\left(\left|\frac{\tilde{u}_2-\tilde{u}_1}{\delta y}\right|^2 + \left|\frac{\tilde{u}_N-\tilde{u}_{N-1}}{\delta y}\right|^2\right)$$

where $\tilde{u}_j = \frac{u_j^{k+1}+u_j^k}{2}$.

Proof. The proof of this proposition follows the same line than that of the continuous case and we omit it.

4.2. Boundary condition for the wave equation

We now focus on the wave equation (2.15) describing the evolution of the fluctuation density of the ions

$$\left(\partial_t^2 - v_s^2\partial_y^2\right)\delta n = \frac{m_e}{4m_i}\frac{k_0^2}{k_{De}^2}\frac{\omega_{pe}^2}{\omega_0^2}\partial_y^2|E|^2 + \frac{m_e}{4m_i}v_s\partial_y^2(|A_0|^2 + |A_R|^2), \tag{4.12}$$

and more particularly on the source term (the ponderomotive force). This source term contains three terms that propagate at different velocities. The first term $\partial_y^2 \mid E|^2$ describes the fluctuation due to the propagation of the longitudinal electronic plasma waves. The second and the third terms $\partial_y^2(|A_0|^2 + |A_R|^2)$ describe the fluctuation of density due to the propagation of the electromagnetic laser field and the Raman backscattered wave. The key point is that in physical applications, the velocity v_s of the acoustic waves is small compared to, the group velocity v_0 of the laser and the group velocity v_R of the Raman field. Moreover the group velocity of electronic plasma waves is also small compared to the electromagnetic waves. Therefore the significant part is

$$\partial_t^2\delta n - v_s^2\partial_y^2\delta n = \partial_y^2 f_0(y - v_0 t) + \partial_y^2 f_R(y - v_R t), \quad 0 \leqslant y \leqslant 1, \tag{4.13}$$

$$\delta n(0, y) = 0, \quad 0 \leqslant y \leqslant 1, \tag{4.14}$$

$$\partial_t\delta n(0, y) = 0, \quad 0 \leqslant y \leqslant 1, \tag{4.15}$$

where $v_0 > 0$, $v_R < 0$ and v_s is a small positive parameter such that $v_s \ll v_0, \mid v_R \mid$. Here, f_0 and f_R are given functions and they refer to the fields A_0 and A_R, respectively. The exact solution of (4.13)–(4.15) reads

$$\delta n(t, y) = \alpha f_0(y - v_s t) + \beta f_0(y + v_s t) + \gamma f_0(y - v_0 t) + \delta f_R(y - v_R t), \tag{4.16}$$

where α, β, γ and δ are real constant.

This explicit solution for δn shows us that the perturbations of density due to the source terms $\partial_y^2 f_{0,R}(y - v_{0,R}t)$ propagate more rapidly than $\alpha f_0(y - v_s t) + \beta f_0(y + v_s t)$. We work on a time scale for the full system for which this perturbation at velocity v_s does not have the time to leave the computational domain. It is therefore sufficient to build absorbing boundary conditions for the perturbations which leave the domain at velocity v_0, respectively v_R at point $y = L$, respectively at point $y = 0$. To ensure this, the boundary conditions for δn consists in our case in the following first order boundary conditions

$$\partial_t\delta n + v_R\partial_y\delta n = 0, \quad y = 0, \tag{4.17}$$

$$\partial_t\delta n + v_0\partial_y\delta n = 0, \quad y = 1. \tag{4.18}$$

In order to validate this kind of boundary condition, we use the scheme introduced by Glassey [10]. It reads

$$\frac{\delta n^{k+1} - 2\delta n^k + \delta n^{k-1}}{\delta t^2} - v_s^2 D_+ D_-\left(\frac{\delta n^{k+1} + \delta n^{k-1}}{2}\right) = D_+ D_-\left(f_0^k + f_R^k\right), \tag{4.19}$$

where the discrete operator D_+D_- is defined by

$$(D_+D_-\delta n)_i = \frac{\delta n_{i+1} - 2\delta n_i + \delta n_{i-1}}{\delta y^2}, \quad i = 2, N-1. \tag{4.20}$$

The quantities $\delta n_1^k, \delta n_N^k$ are given by the following discretization of the boundary conditions (4.17) and (4.18) at each time step k

$$\delta n_1^{k+1} = \left(1 + \frac{v_R\delta t}{\delta y}\right)\delta n_1^k - \frac{v_R\delta t}{\delta y}\delta n_2^k, \tag{4.21}$$

$$\delta n_N^{k+1} = \left(1 - \frac{v_0\delta t}{\delta y}\right)\delta n_N^k + \frac{v_0\delta t}{\delta y}\delta n_{N-1}^k. \tag{4.22}$$

For the numerical illustrations of this problem, we take $v_s = 0.15$, $v_0 = 0.9$, $v_R = -0.8$, $f_{0,R}(t, y) = 0.02e^{-\frac{\left(y-\frac{1}{2}-v_{0,R}t\right)^2}{2}}$, $N = 1024$ and $\delta t = \delta y \min\left(\frac{1}{v_0}, \frac{1}{|v_r|}\right)$. The initial conditions n_0 and n_1 are set to zero.

On Fig. 2, we can see the evolution of the density fluctuation with time. At the beginning of the simulation, a perturbation due to the force f_0, f_R causes a sink of density. This perturbation propagates at four velocities which are $v_R, -v_s, v_s, v_0$. It is obvious that the perturbations propagating at velocity v_R, v_0 go more quickly than the others propagating at velocity $-v_s, v_s$. The part of the perturbation traveling at velocity v_R (v_0) leaves the simulation box at point $y = 0$ ($y = 1$) (see Fig. 2). The perturbations going at velocity $\pm v_s$ still propagate.

Remark 4.2. At this point, we gave some effective absorbing boundary conditions for a linear Schrödinger equation and for a wave equation. For the linear Schrödinger equation endowed by the boundary condition (4.3), we found an estimate which

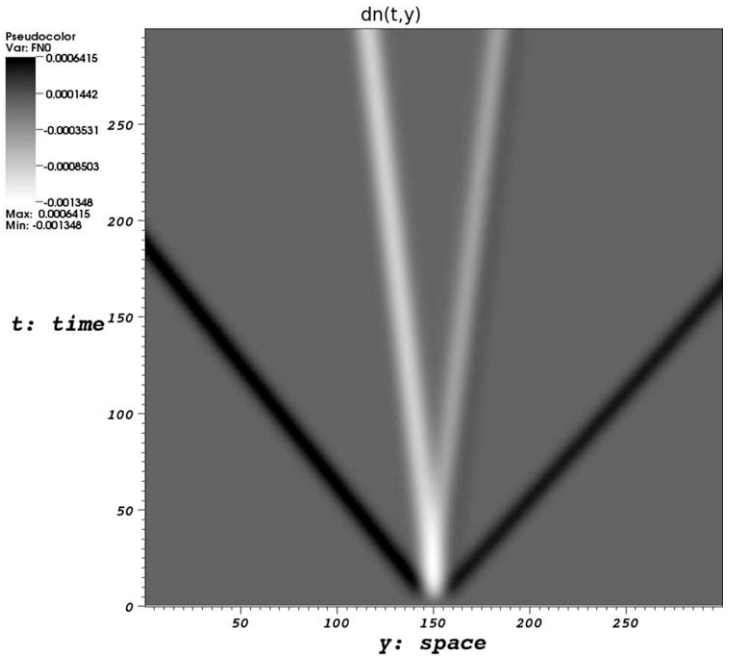

Fig. 2. Spatio-temporal evolution of the density fluctuation δn solution of (4.13)–(4.15) endowed with the boundary conditions (4.17) and (4.18).

shows us that the energy of the solution decrease with time. Unfortunately, we are not able to give such a theoretical result on a nonlinear version of this kind of system. Nevertheless, in the next part, we show that we can apply this kind of boundary conditions on a Zakharov model with a satisfactory numerical accuracy.

4.3. The boundary conditions for the Zakharov system

Using the boundary conditions for the Schrödinger equation and for the wave equation, we obtain the following Zakharov model

$$i(\partial_t u + v\partial_y u) + \varepsilon\partial_y^2 u = nu, \quad 0 < y < 1, \tag{4.23}$$

$$\partial_t^2 \delta n - v_s^2 \partial_y^2 \delta n = \partial_y^2(|u|^2), \quad 0 < y < 1, \tag{4.24}$$

$$u(0,y) = u_0(y), \tag{4.25}$$

$$u(t,0) = 0, \tag{4.26}$$

$$\partial_t u + v\partial_y u = 0, \quad y = 1, \tag{4.27}$$

$$\delta n(0,y) = 0, \quad \partial_t \delta n(0,y) = 0, \tag{4.28}$$

$$\partial_t \delta n + v\partial_y \delta n = 0, \quad y = 1. \tag{4.29}$$

Even if we are not able to justify rigorously our set of boundary conditions for the full Zakharov system (4.23)–(4.29), the numerically accuracy is satisfactory. Indeed, in Fig. 3, we have plotted the modulus of electric field u and the variation of density δn with respect to time. As seen on the snapshots, no visible reflexions can be seen on any of the curves. For the simulation described in Fig. 3, we have taken $\delta t = \delta y = 0.01$. Of courses, these results has to be confirmed on the complete system

For the whole system, we therefore consider the following set of boundary conditions to

$$\partial_t A_0 + v_0\partial_y A_0 = 0, \quad y = L, \tag{4.30}$$

$$\partial_t A_R + v_R\partial_y A_R = 0, \quad y = 0, \tag{4.31}$$

$$\partial_t \delta n + v_0\partial_y \delta n = 0, \quad y = L, \tag{4.32}$$

$$\partial_t \delta n + v_R\partial_y \delta n = 0, \quad y = 0. \tag{4.33}$$

Concerning the plasma waves, since the group velocity of the electronic plasma waves is small with respect to v_0 and v_R (see [5,6]), we use periodic boundary condition for E, that is $E(0) = E(L)$. These boundary conditions are discretized as we described previously using a spectral method.

The detailed numerical results are given in the next section.

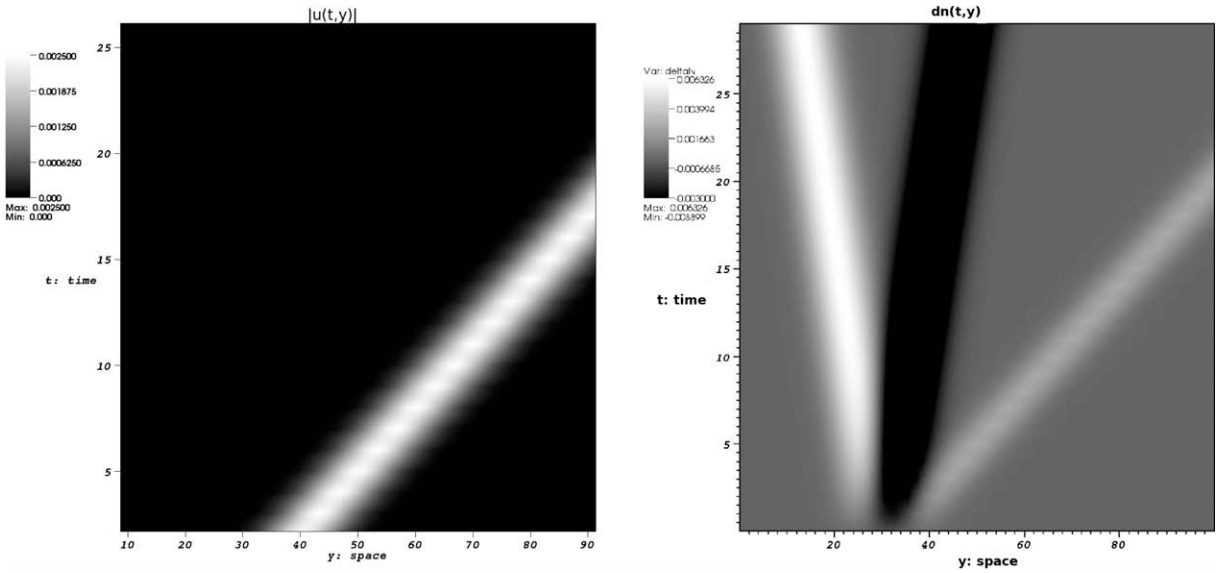

Fig. 3. Spatio-temporal evolution of $|u|(t,y)$ (left) and $\delta n(t,y)$ (right) solution of (4.23) and (4.29) for $\varepsilon = 5 \cdot 10^{-3}$.

5. Numerical results

The numerical computations are obtained with the dimensionless system (2.12)–(2.18) where the time unit is $T = \frac{1}{\omega_0}$, the space unit is $L = k_0 = \frac{1}{\lambda_0}$ and the velocity unit is $V = v_{the} = \omega_{pe}\lambda_{De}$.

The physical parameters that we use until the end of this section are the following ones. They are representative of the physics that is involved [13,14].

- the velocity of light is $c = 3 \cdot 10^8$ m s^{-1},
- the thermal velocity of electrons is taken to be equal to $v_{the} = 0.1c$,
- the mass ratio is taken to be $\frac{m_e}{m_i} = \frac{1}{2000}$,
- the sound velocity is $c_s = \sqrt{\frac{m_e}{m_i}} v_{the}$,
- the plasma frequency $\omega_{pe} = 3 \cdot 10^{15}$ s^{-1},
- the wave number of the laser field $k_0 = 3 \cdot 10^6$,
- the Debye's length $\lambda_{De} = \frac{v_{the}}{\omega_{pe}} = 10^{-8}$ m.

With this parameters, we compute the frequency ω_0 thanks to the dispersion relation

$$\omega_0 = \sqrt{\omega_{pe}^2 + k_0^2 c^2}.$$

The others parameters k_R, k_1, ω_R and ω_{1d} are computed using the following matching conditions for the three-waves resonance condition:

$$k_0 = k_R + k_1, \quad \omega_0 = \omega_R + \omega_{pe} + \omega_{1d},$$

where

$$\omega_R = \sqrt{\omega_{pe}^2 + k_R^2 c^2}, \quad \omega_{1d} = \frac{2}{\delta t} \arctan\left(\alpha \delta t \frac{1 - \cos(k_1 \delta y)}{\delta y^2}\right),$$

where $\alpha = \frac{3k_0^2}{2k_{De}^2}$.

We will perform the computations of the solution of system (2.12)–(2.18) on the spatial domain $[0, Ly]$ with $Lk_0 = 250$.

For the initial conditions, we consider a gaussian initial data for A_0 of the form

$$A_0(0,x) = 0.3e^{-0.01(x-40)^2}.$$

In the context of simulated Raman instability, a non-zero initial datum is needed on A_R in order to start the instability and we take $A_R(0,x) = 0.005A_0(0,x)$. Furthermore, E, δn and $\partial_t \delta n$ are taken equal to 0 at time $t = 0$. The initial electron distribution function is assumed to be a Maxwellian:

$$F_e(0,v) = \frac{1}{\sqrt{2\pi}} e^{-\frac{v^2}{2}},$$

which gives the following initial condition for the Landau damping rate

$$\hat{v}(0,\xi) = \sqrt{\frac{\pi}{8}}\frac{k_{De}^3}{k_0^3}\frac{1}{|\xi|^3}e^{-\frac{k_{De}^2}{2k_0^2\xi^2}}.$$

The number of discretization points in space is $N_y = 2048$ and we choose $\delta t = \delta y \min\left(\frac{1}{v_0}, \frac{1}{|v_r|}\right)$.

We perform the simulation on the time interval $[0, T_{\max}]$ with $T_{\max} = 100$.

This section is splitted in two parts. In the first one, we provide some numerical validation of the use of our set of boundary conditions and of the numerical dispersion relation. In the second part, we perform a typical computation and we compare our results to two previous studies in order to emphasize the novelties of our approach.

5.1. Numerical validation

For the Schrödinger part of the Zakharov type systems, the use of Neuman boundary conditions instead of absorbing ones give rise to reflections that change deeply the results of the computations. However, it is not clear that this effect still exist for the complete system (2.12)–(2.15). We perform two tests that show that one has to use absorbing boundary conditions for A_0, A_R and δn in order to avoid the effects of reflections. In the first test case, we use Neuman boundary conditions for A_C and A_R and we keep the absorbing boundary conditions (4.17) and (4.18) for the fluctuation of density δn. We compare the

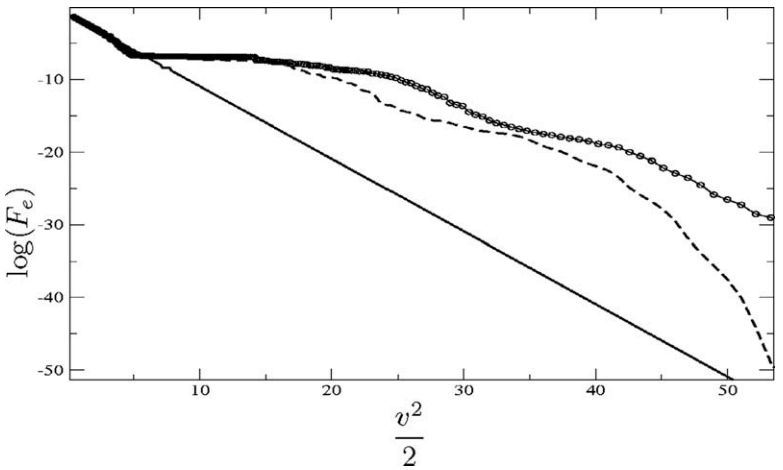

Fig. 4. The log of the spatially averaged electron distribution function F_e as a function of kinetic energy $\frac{v^2}{2}$ at initial time (solid line) and at the end of simulation $t = 100$: the circle point corresponds to the Neumann boundary conditions on A_0 and A_R and the dashed line corresponds to the our boundary conditions.

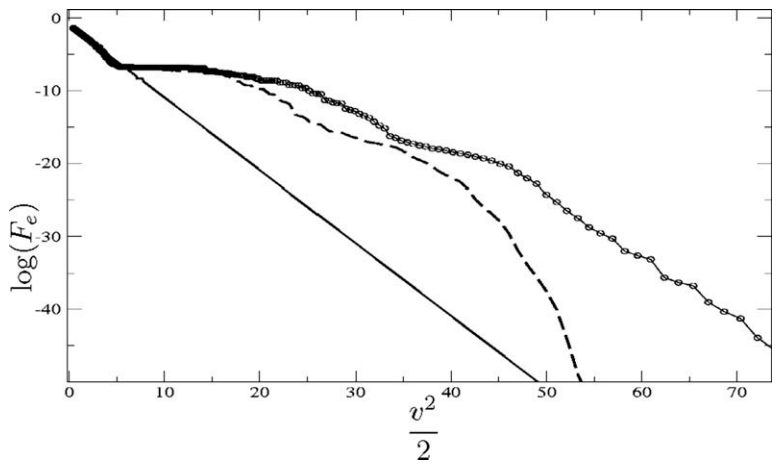

Fig. 5. The log of the spatially averaged electron distribution function as a function of the kinetic energy $\frac{v^2}{2}$ at initial time (solid line) and at the end of simulation: the circle point corresponds to the Neumann boundary condition on δn and the dashed line corresponds our to the boundary conditions.

result with that of the computation made with the whole set of absorbing boundary conditions (4.30)–(4.33). The results are given in Fig. 4. We have plotted the log of the spatially average electron distribution F_e as a function of the kinetic energy $\frac{v^2}{2}$ at the initial time (solid line) and at the end of the simulation: the circle points correspond to the Neuman boundary conditions on A_0 and A_R; the dashed line corresponds to the absorbing boundary conditions (4.27). The inverse of the slop of this curve for large values of $\frac{v^2}{2}$ is the temperature of accelerated electrons. It is clear that the use of Neuman boundary conditions for A_0 and A_R overestimate this temperature.

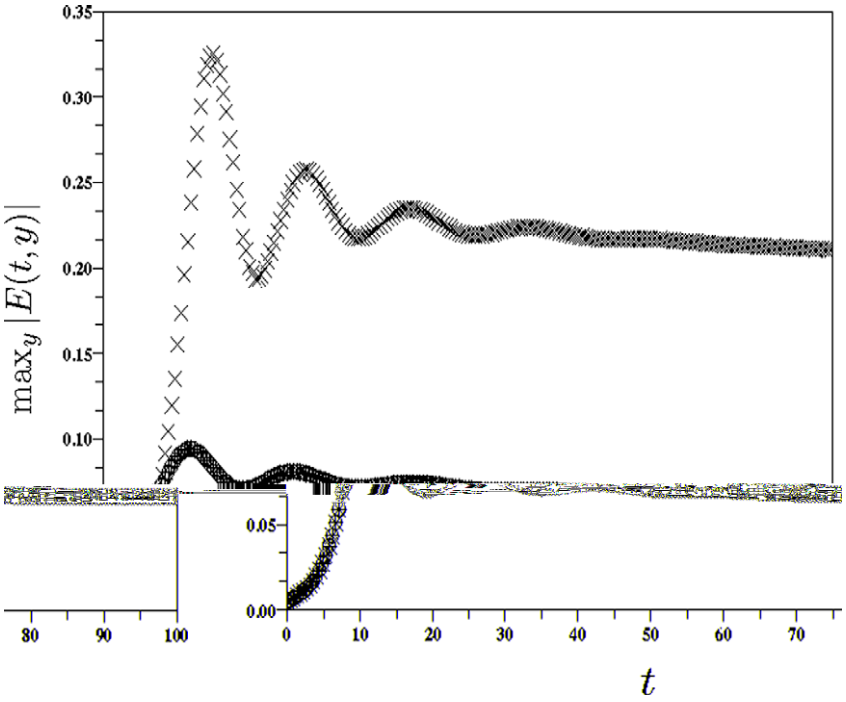

Fig. 6. $\max_{y\in[0,L]} |E(t,y)|$ as a function of time. The crossed-line correspond to the numerical dispersion relation, and the circle line correspond to the theoretical dispersion relation.

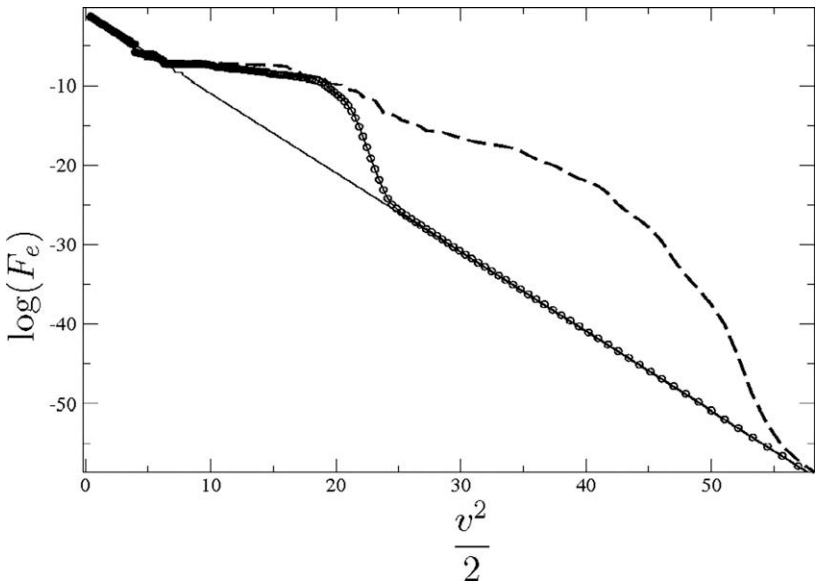

Fig. 7. The log of the spatially averaged electron distribution function F_e as a function of the kinetic energy, for the numerical dispersion relation (dashed line) and for the theoretical dispersion relation (circle line).

In the second test case, we use absorbing boundary conditions for A_0 ans A_R but Neuman boundary conditions for δn. The result is plotted in Fig. 5. Again, the temperature is overestimated.

It is therefore necessary to use absorbing boundary conditions.

The last point that we want to emphasize is the use of the discrete dispersion relation. We have performed two computations, the first one using the numerical dispersion relation (3.21), the second one using the continuous one (2.11). The results are given in Figs. 6 and 7. In Fig. 6, we have plotted $\max_{y\in[0,L]} \mid E \mid (t,y)$ as a function of time for both dispersion relations. The crossed-line correspond to the numerical dispersion relation and the circle one to the continuous one.

In the case where we used the continuous dispersion relation, the discretization of $A_R^* A_0 e^{i(k_1 y-\omega_1 t)}$ is not resonant with the discretization of the linear part of (2.14). This means that, the amplitude of the electronic plasma waves does not reach the necessary threshold to develop the Raman instability [14] and we stay in a linear regime where the Landau damping phenomena plays no role on the saturation level of the electronic plasma waves. It is the reason for which the continuous relation does not give the right saturation level for the electronic plasma waves.

In the case where we used the discrete dispersion relation, the discretization of $A_R^* A_0 e^{i(k_1 y-\omega_1 t)}$ is resonant with the discretization of the linear part of (2.14). So the amplitude of the electronic plasma waves reaches the threshold to start the Raman instability and the exchange of energy between the electronic plasma waves and the electrons (Landau damping) can occurs.

On Fig. 7, we have plotted the log of the spatially average electron distribution function as a function of the kinetic energy for both dispersion relations. The use of the continuous dispersion relation induces an underestimate of the electron heating. It is therefore necessary to use the discrete dispersion relation.

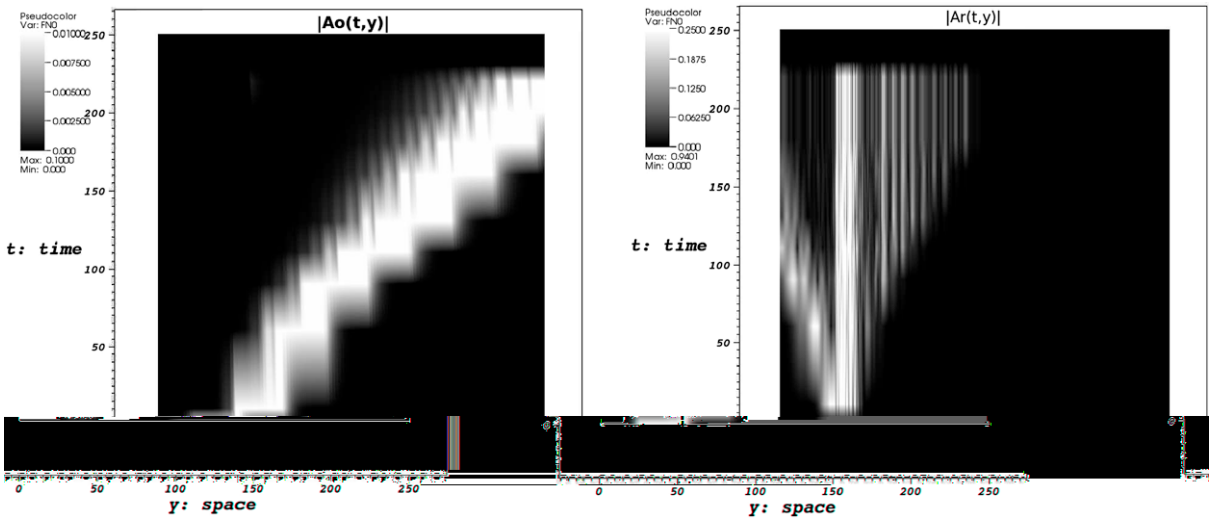

Fig. 8. Spatio-temporal evolution of the modulus of the normalized potentials A_0 and A_R: $\mid A_0 \mid (t,y)$ (left) and $A_R(t,y)$ (right) solutions of the full system.

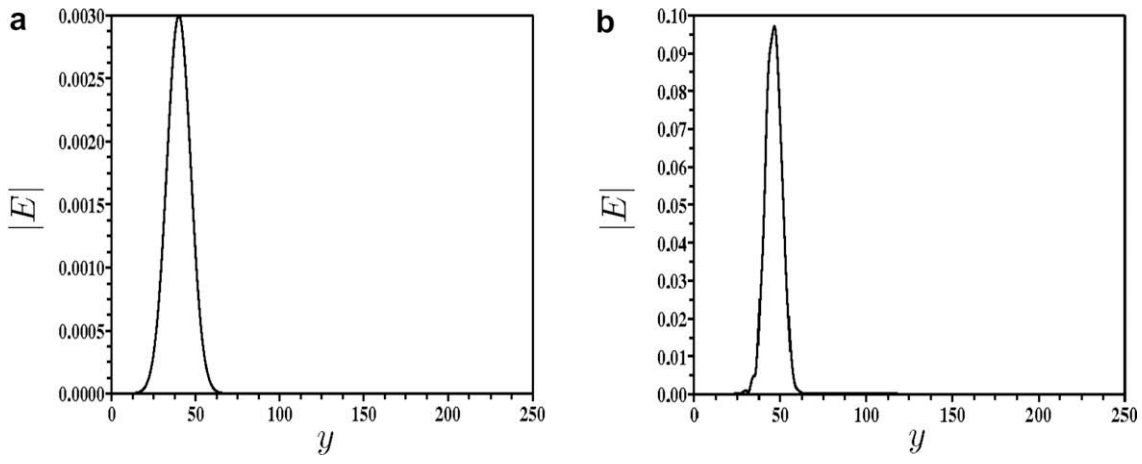

Fig. 9. Snapshots of the modulus of the electronic plasma waves E at time $t = 10n$ for $n = 1$ (a), $n = 10$ (b) in the resonant case.

5.2. Reference test case and comparison to previous models

We present in Figs. 8 and 9 the spatio-temporal evolution of the modulus of the fields A_0, A_R, E. As indicated before A_0 moves to the right with a positive velocity. A_R moves to the left because it has a negative velocity while E is stationary.

In Fig. 10, one can compare the time evolution of the L^2-norm of the fields. For A_R and E, one has a rapid growth corresponding to the Raman instability followed by a saturation stage. In Fig. 7 (dashed line), we have plotted the spatially averaged electron distribution function of the kinetic energy at the end of the simulation. One can observe a significant heating of the electrons (the temperature is given by the inverse of the slop of the curve).

At the beginning of simulation, the laser field and the stimulated Raman field interact in order to create an electronic plasma waves. These three fields combine in order to create a perturbation on the low-frequency density δn. The laser field propagates on the positive y-direction and create on its way Raman backscattered wave which propagate on the y-negative direction. Concerning the evolution of the spatial profile of the electronic plasma wave created by the three wave resonance, we can see that its amplitude grows with time and therefore this confirms that its velocity is small with respect to that of A_R and A_0 as can be seen in its dispersion relation.

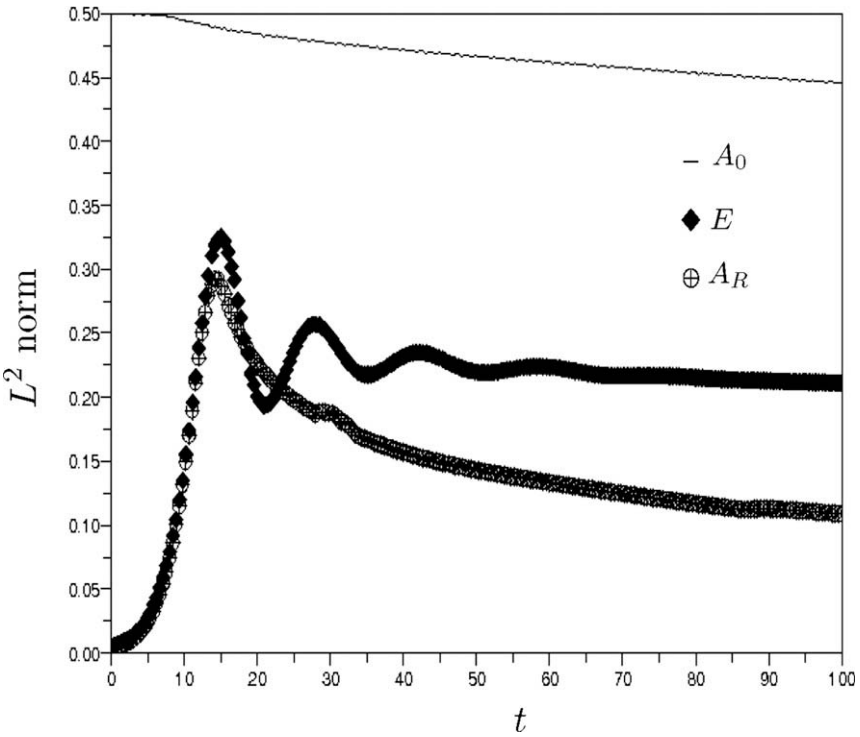

Fig. 10. L^2 norm in function of time for A_0 corresponding to the solid line, A_R corresponding to the circle points and E corresponding to the square line.

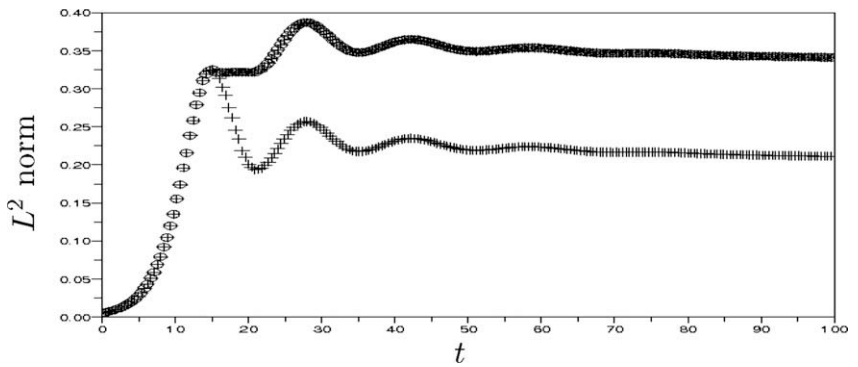

Fig. 11. The L^2 norm of $|E|$ in function of time without Landau damping (circle line) and with Landau damping (dotted line) by using the numerical dispersion relation.

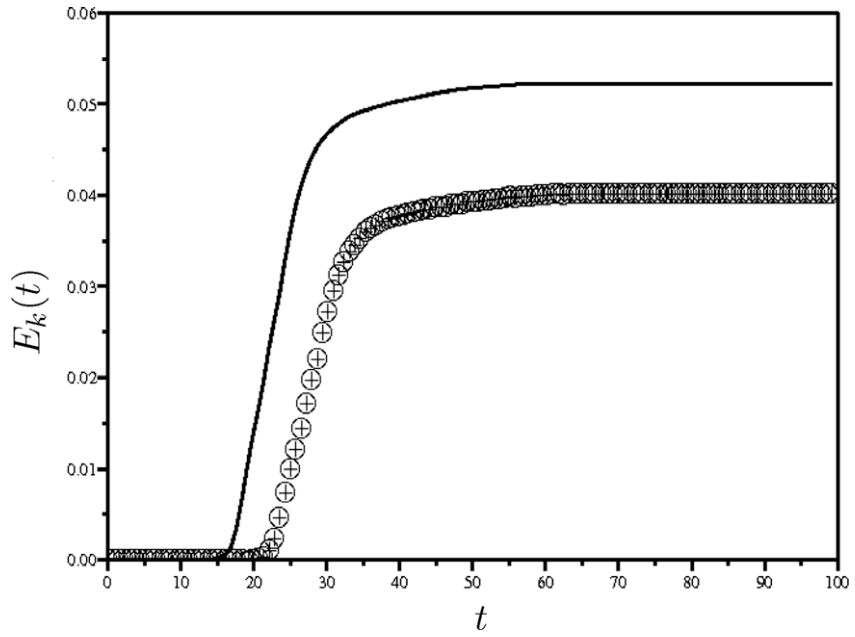

Fig. 12. Time evolution of the electron kinetic energy $E_k(t) = \frac{1}{2}\int v^2 F_e(t,v)dv - \frac{1}{2}$ for the full system (circle line) and for fixed A_0, A_R (solid line).

The Fig. 10 shows that there are some energy exchanges between the different fields. In a first stage, there is a transfer of energy from the laser field to the Raman field and to the electronic plasma waves until an amplification threshold is reached. This stage occurs before time $\omega_0 t = 15$.

In a second stage, the evolution becomes nonlinear and the Landau damping acts. A new plasma waves is created and a transfer of energy between this plasma wave and the electrons take place. This lead to a creation of hot electron tail as can be seen on the Fig. 10. The saturation level of the Raman begins to decrease.

Our model is therefore able to describe the main feature of this coupling. We now compare our result with two previous models. The first model is the Raman instability without Landau damping [6]. The result is given in Fig. 11. The saturation threshold for the electronic plasma waves is lower if we take into account the landau damping that allows transfers of energy from the electronic plasma waves to the accelerated electrons.

The second model is the Landau damping ones used in [2]. It consists in fixing A_0 and A_R and keeping only Eq. (2.14). The result is given in Fig. 12. We have plotted the electron energy $\frac{1}{2}v^2 F_e(t,v)dv - \frac{1}{2}$ as a function of time for both systems. The Landau system of [2] overestimate the transfer of energy to the accelerated electrons.

6. Conclusion

In this paper, we have introduced a new system describing the coupling of the landau damping and the Raman amplification. We have proposed a numerical scheme and proved its L^2 stability.

We have provided a set of boundary conditions and we have showed numerically that they are necessary to obtain accurate results. The Raman instability relies on a three-waves interaction condition. We have introduced a numerical dispersion relation and we have validated it.

We have compared our results with two previous models and we obtain a more reliable simulation of the main features of this complex physical process, without using kinetic-type models.

Further development should concern a multi-D version of the Landau damping as well as the construction of intermediate models between full Vlasov–Maxwell and the one considered here.

References

[1] X. Antoine, C. Besse, S. Descombes, Mathematical and numerical analysis of nonlinear artificial boundary conditions for the one-dimensional Schrödinger equation, SIAM J. Numer. Anal. 43 (2006) 2272–2293.
[2] R. Belaouar, T. Colin, G. Gallice, C. Galusinski, Theoritical and numerical study of a quasi-linear Zakharov system describing Landau damping, M2AN Math. Model. Numer. Anal. 40 (6) (2006) 961–990. 2007.
[3] R. Belaouar, T. Colin, G. Gallice, V. Tikhonchuk, Quasi-linear electron acceleration in a driven plasma wave, Plasma Phys. Control. Fusion 49 (2007) 969984.
[4] C. Besse, Schéma de relaxation pour l'équation de Schrödinger non linéaire et les systèmes de Davey et Stewartson, C.R. Acad. Sci. Paris. Sér. I Math. 326 (1998) 1427–1432.
[5] M. Colin, T. Colin, On a quasi-linear Zakharov System describing laser-plasma interactions, Differen. Integral Eqs. 17 (3–4) (2004) 297–330.

[6] M. Colin, T. Colin, A numerical model for the Raman amplification for laser-plasma interaction, J. Comput. Appl. Math. 193 (2) (2006) 535–562.
[7] J-L. Delcroix, A. Bers, Physique des plasmas 1, 2. Inter Editions–Editions du CNRS, 1994.
[8] P. Degond, Spectral theory of the linearized Vlasov–Poisson equation, Trans. Am. Math. Soc. 294 (2) (1986) 435–453.
[9] L. Di Menza, Transparent and artificial boundary conditions for the linear Schrödinger equation, Numer. Funct. Anal. Optim. 18 (7–8) (1998) 759–776.
[10] R.T. Glassey, Convergence of an energy-preserving scheme for the Zakharov equations in one space dimension, Math. Comput. 58 (197) (1992) 83–102.
[11] R.T. Glassey, J. Schaeffer, On time decay rates in Landau damping, Commun. Partial Differen. Eqs. 20 (3–4) (1995) 647–676.
[12] Thomas Hagstrom, Radiation boundary conditions for the numerical simulation of waves, Acta Numer. 8 (1999) 47–106.
[13] G. Riazuelo, Etude théorique et numérique de l'influence du lissage optique sur la filamentation des faisceaux lasers dans les plasmas sous-critiques de fusion inertielle. Thèse de l'Université Paris XI, 1999.
[14] D.A. Russel, D.F. Dubois, H.A. Rose, Nonlinear saturation of simulated Raman scattering in laser hot spots, Phys. Plasmas 6 (4) (1999) 1294–1317.
[15] K.Y. Sanbomatsu, Competition between Langmuir wave–wave and wave–particle interactions, Thesis of University of Colorado, Department of Astrophysical, 1997.
[16] K.Y. Sanbomatsu et al, The effect of kinetic processes on Langmuir turbulence, Phys. Plasmas 7 (2000) 1723.
[17] K.Y. Sanbomatsu et al, Quantitative comparison of reduced-description particle-in-cell and quasi-linear–Zakharov models for parametrically excited Langmuir turbulence, Phys. Plasmas 7 (2000) 2824.